ELSEVIER

Chemical Engineering Journal 116 (2006) 123–132

Chemical Engineering Journal

www.elsevier.com/locate/cej

Development of a microchannel reactor concerning steam reforming of methanol

Xinhai Yu*, Shan-Tung Tu, Zhengdong Wang, Yunshi Qi

School of Mechanical and Power Engineering, East China University of Science and Technology, Shanghai 200237, China

Received 7 February 2005; received in revised form 11 November 2005; accepted 23 November 2005

Abstract

To develop a portable power device using fuel cell technology, the miniaturization of the hydrogen production unit is indispensable. In this paper, preparation of a microchannel reactor concerning steam reforming of methanol (SRM) has been investigated by optimizing the parameters of diffusion bonding and the composition of catalyst coatings. The results show the microchannel reactor can be sealed successfully by diffusion bonding at the optimized parameters (900 °C, 20 MPa, 1 h). The most active and selective catalyst coating is Cu50/Zn50 [Ce5] (Cu/Zn/Ce = 50/50/5, molar). It has been found that CeO_2 has an important influence on improving catalytic activity, decreasing the outlet CO concentration, and strengthening the stability. Based on the characterization of catalyst coatings, it can be attributed to the increase in copper area and to the change in oxidation state of copper that results in the synergetic effect of Cu^0 and Cu^+. In addition, the effects of reaction temperature, space velocity, molar ratio of methanol to water, and reaction time were also investigated in the developed microchannel reactor with the Cu50/Zn50 [Ce5]. The results show that the microchannel reactor can generate enough hydrogen for a power output of 11 W.

Keywords: Microchannel; Diffusion bonding; Catalyst; Coating; Steam reforming of methanol

1. Introduction

Today fuel cells are considered as environment friendly and high efficiency systems for the production of electricity. Worldwide research efforts have been made to the improvement of the technology [1]. A proton exchange membrane (PEM) fuel cell system has been considered to be suitable for vehicles and portable applications [2]. The fuel cells need hydrogen or hydrogen-rich feed gas as fuel. Hydrogen for fuel cells can be produced in mobile units by steam reforming of methanol (SRM) because of methanol's low reforming temperatures, good miscibility with water, and low content of sulfur compounds [3]. The main reactions in the proposed route may be represented by the following equations.

Steam reforming of methanol:

$$CH_3OH + H_2O \Leftrightarrow CO_2 + 3H_2 \quad \Delta H^0_{298} = +49.4\,\mathrm{kJ\,mol^{-1}} \tag{1}$$

Methanol decomposition:

$$CH_3OH \Leftrightarrow 2H_2 + CO \quad \Delta H^0_{298} = +92.0\,\mathrm{kJ\,mol^{-1}} \tag{2}$$

Water-gas shift reaction:

$$CO + H_2O \Leftrightarrow CO_2 + H_2 \quad \Delta H^0_{298} = -41.1\,\mathrm{kJ\,mol^{-1}} \tag{3}$$

Microchannel reactors are much more suitable for the distributed production of hydrogen compared to conventional systems [4]. With typical channel widths of 100–1000 μm [5,6], the large surface-to-volume ratios in these reactors lead to good heat and mass transfer properties and hence process intensification [7]. Microchannel reactors work under laminar flow conditions demonstrating low-pressure drop compared to randomly fixed-bed. The short radial diffusion time in gas phase leads to narrow residence time distribution of gases. This allows optimizing the contact time of reactors avoiding the formation of unwanted by-products. Moreover, the short residence time allows a quick response to dynamic changes in the inlet conditions [8,9]. For non-stationary operations of the reactor, this feature is essential.

Recent efforts in the area of microreaction technology have shown promising results. Pfeifer et al. studied microstructured reactors with small channels (100 μm × 100 μm) and applied

* Corresponding author. Tel.: +86 21 64252363; fax: +86 21 64251804.
E-mail address: yxhh@ecust.edu.cn (X. Yu).

1385-8947/$ – see front matter © 2005 Elsevier B.V. All rights reserved.
doi:10.1016/j.cej.2005.11.008

dispersed ZnO nanoparticles to the microchannel walls [10]. A 40 W equivalent microchannel fuel processor operating on methanol was successfully developed by Pacific Northwest National Laboratories (PNNL). The fuel processor consists of a vaporizer, steam reformer, and recuperative heat exchanger with the active system weighing less than 80 g [11]. Chen et al. [12] developed a microchannel reactor for CO preferential oxidation (PROX) with potassium on supported RH metal catalysts. Park et al. [3] fabricated a microchannel reactor with dimensions of 70 mm × 40 mm × 30 mm concerning steam reforming of methanol. The results show the fuel processor generates enough hydrogen for power output of 15 W.

However, the microchannel technology still has a long way to go in high reliability for long-period operation and low cost of fabrication. Especially, most microchannel reactors were developed by the method of glue bonding, which is inconvenient and costly for large-scale manufacturing. In addition, more detailed studies are also needed in the optimization of the preparation procedure and the composition of the catalyst coatings, since high catalytic activity and selectivity of the catalyst coatings are crucial to the application of microchannel reactors in fuel cells.

In this paper, preparation of a microchannel reactor concerning SRM has been investigated by optimizing the parameters of diffusion bonding and the composition of catalyst coatings. During the optimization of catalyst coatings, an annular micro-reactor was used due to its similarity of annular micro-reactors to microchannel reactors in flow pattern, simplicity of fabrication, and repeated usage. The performances of the bonded microchannel reactor with the optimized catalyst coating at various operating conditions have also been studied.

2. Experimental

2.1. Microchannel reactor fabrication

A schematic sketch of the annular micro-reactor is reported in Fig. 1. The reactor consists of an internal cylinder coaxially placed in an external tube. The gas flows downwards the annulus between the cylinder and the tube. The gap of the annulus is kept constant at 0.5 mm.

The two reactors are both made of aluminium-contained stainless steel (DIN 1.4767, “Fe–Cr–Al”). Microchannels were patterned on the Fe–Cr–Al sheets by electric spark processing. Three types of patterned sheets were prepared to construct a base structure. The thickness of metal sheet was 780 μm. A cover sheet (Fig. 2a) has one hole, which acts as a flow path. A manifold sheet (Fig. 2b) has one triangular manifold for enhancing the uniform distribution of flow through each microchannel. A microchannel sheet (Fig. 2c) has parallel channels of a rectangular shape on it. The microchannel is 1000 μm wide, 600 μm deep, and 32 mm long. The configuration of a base structure consists of two cover sheets, six manifold sheets and five microchannel sheets. Surfaces of all sheets in three types were polished to a roughness of 2 μm followed by cleaning in acetone prior to diffusion bonding. Fig. 3 shows the wedded unit of the microchannel reactor. The dimensions of the microchannel reactor are about 40 mm × 40 mm × 9.78 mm, respectively. The effective volume of microchannel reactor is 2.4 cm^3, including microchannel and triangular inlet and outlet zone as well.

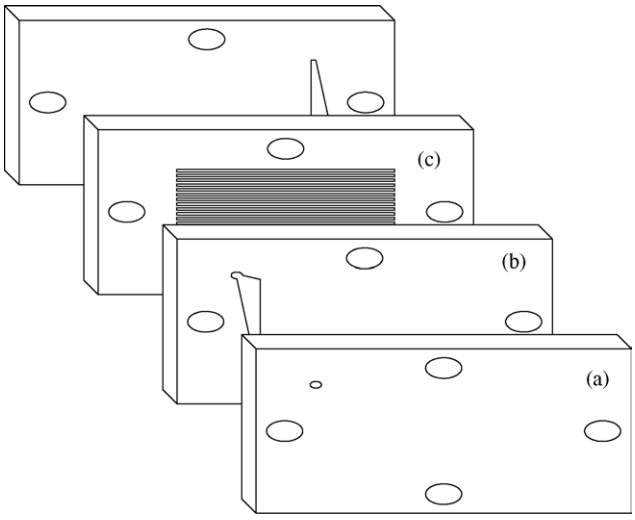

Fig. 2. Representative configuration of base structure.

2.2. Catalyst coating preparation

The two reactors are both made of aluminium-contained stainless steel (DIN 1.4767, “Fe–Cr–Al”). By heating the alloy for approximately 5 h at 1000 °C, a thin alumina film was formed on the surface [13]. This Al_2O_3 film greatly improves the adherence of the catalyst layers on the walls of the micro-reactors. The two reactors were initially coated with aluminum oxide (γ-Al_2O_3) to increase the surface area and to enable dispersion of the catalytic material. A γ-Al_2O_3 powder with surface area of 185 $m^2\,g^{-1}$ was ball milled for 24 h and was subsequently added slowly into the solution of nitric acid with concentration of 2 mol L^{-1} under stirring to prepare γ-Al_2O_3 slurry. After

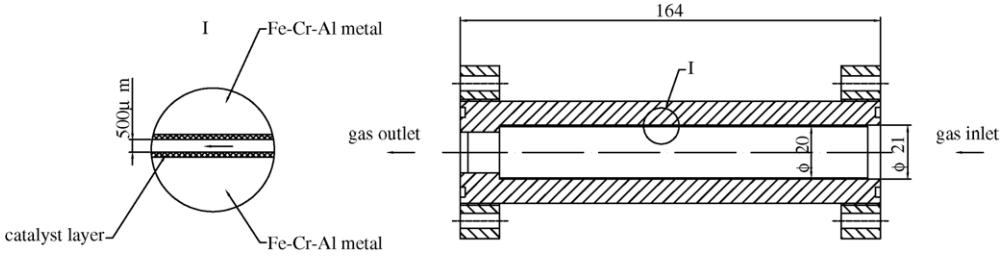

Fig. 1. Schematic diagram of the annular micro-reactor.

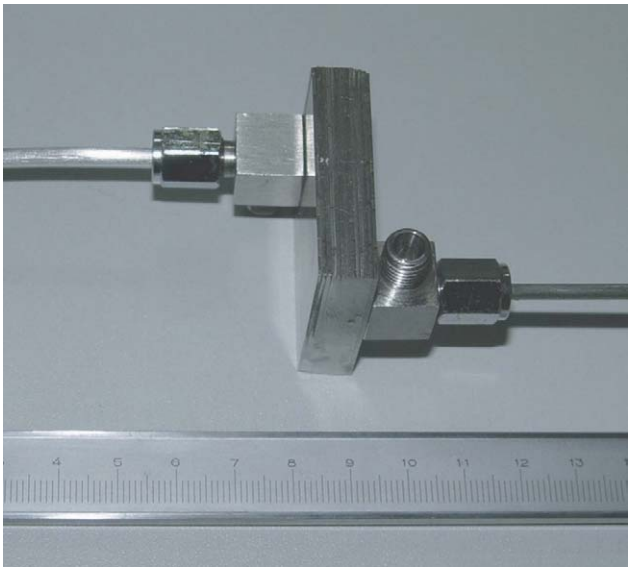

Fig. 3. The microchannel reactor.

being stirred for 30 min, the slurry was aged up to 2 h. Then, the γ-Al_2O_3 slurry was deposited on the walls of the annular micro-reactor and microchannel reactor. After being dried in air and subsequently calcined at 500 °C, the γ-Al_2O_3 coating was formed as support for catalytically active components. Copper and zinc oxides were then deposited by impregnation of the γ-Al_2O_3 coating with an aqueous solution of $Cu(NO_3)_2{\cdot}3H_2O$, $Zn(NO_3)_2{\cdot}6H_2O$, $Ce(NO_3)_3{\cdot}6H_2O$ (analytic grade). The catalyst coating was dried at 120 °C in air for 2 h and subsequently calcined at 450 °C for 4 h unless. The catalyst coating thus prepared by the impregnation method is hereafter denoted as Cu/Zn [Ce], where the numerical values indicate the molar ratio of Cu, Zn and Ce.

2.3. Experimental set-up

The experimental set-up is shown in Fig. 4. It includes a methanol–water supply and evaporator/super-heater unit.

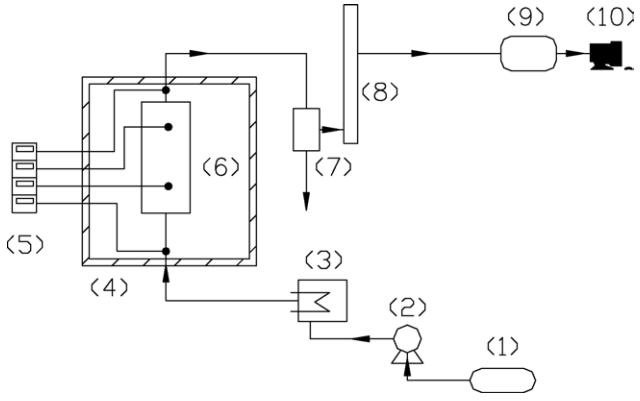

Fig. 4. Laboratory reactor system: (1) fuel tank (deionized water and 99.9% methanol); (2) pump (LEWA); (3) evaporators; (4) oven; (5) thermocouple; (6) annular micro-reactor or microchannel reactor; (7) cooler; (8) flow meter; (9) varian gas chromatograph (FID and TCD detectors); (10) computer with GC evaluation software.

Before entering the annular or microchannel reactor, the liquid methanol–water mixture was fed from the storage tank into the evaporator by a piston membrane metering pump (LEWA metering pump type EK-horizontal with worm gear and flange motor). The annular micro-reactor or microchannel reactor was placed in an electrically heat furnace. The temperature of the furnace was controlled by a PID-temperature-controller with a K-type thermocouple inserted in the furnace. Two E-type thermocouples were mounted on the external wall of the annular micro-reactor or microchannel reactor. Another two E-type thermocouples were placed at the inlet and outlet of the two reactors. The product stream composition was measured using a gas chromatograph from Varian equipped with both TCD and FID detectors. The experiments were carried out over a temperature interval of 220–300 °C. Before reaction, the catalysts were pre-reduced at 280 °C using 10% H_2 in N_2 flowing at 300 $cm^3\,min^{-1}$ for 2 h.

2.4. Characterization

The specific area of the various samples was measured according to the Brunauer–Emmer–Teller theory (BET) by nitrogen adsorption using a Micrometrics ASAP 2010 instrument.

The surface area of copper (S_{Cu}) was determined by applying a nitrous oxide method as described by Osinga et al. [14] and Evans et al. [15] using a micromeritics TPD/TPR 2910 Autochem instrument.

The catalyst samples were analyzed using a JEOL JSM 6360M scanning electron microscope (SEM) equipped with a EDAX FALCON energy dispersive X-ray spectrometry (EDS) unit.

The crystal phase was identified by means of X-ray powder diffraction (XRD) using a BRUKER D8 ADVANCE equipped with a XRK high-temperature chamber. Patterns were obtained during in situ reduction steps. The catalyst coatings were exposed to 5% H_2 in Ar flowing at 80 sccm and diffraction patterns were recorded at selected temperature beginning at 25 up to 280 °C. In these experiments, the temperature was ramped between measurements at a rate of 5 °C min^{-1} with a 5-min pause at each temperature before recording the pattern. The Cu(1 1 1) peak was employed to calculate Cu crystallite size using the Debye–Sherer equation at a scanning rate of 0.42° min^{-1} from 33° to 38°.

X-ray photoelectron spectra (XPS) were recorded using a VG Scientific XPS with a Mg anode operating at 14 kV and 10 mA. Post reaction samples were sealed in He before the sample temperature was lowered to room temperature.

3. Results and discussion

3.1. Effects of diffusion bonding parameters

Micrographs of the interface of the diffusion bonded zone for Fe–Cr–Al alloy sheets at different temperatures and pressures are shown in Fig. 5. The effects of temperature on the percentage of bonded area at a fixed pressure (10 MPa) are

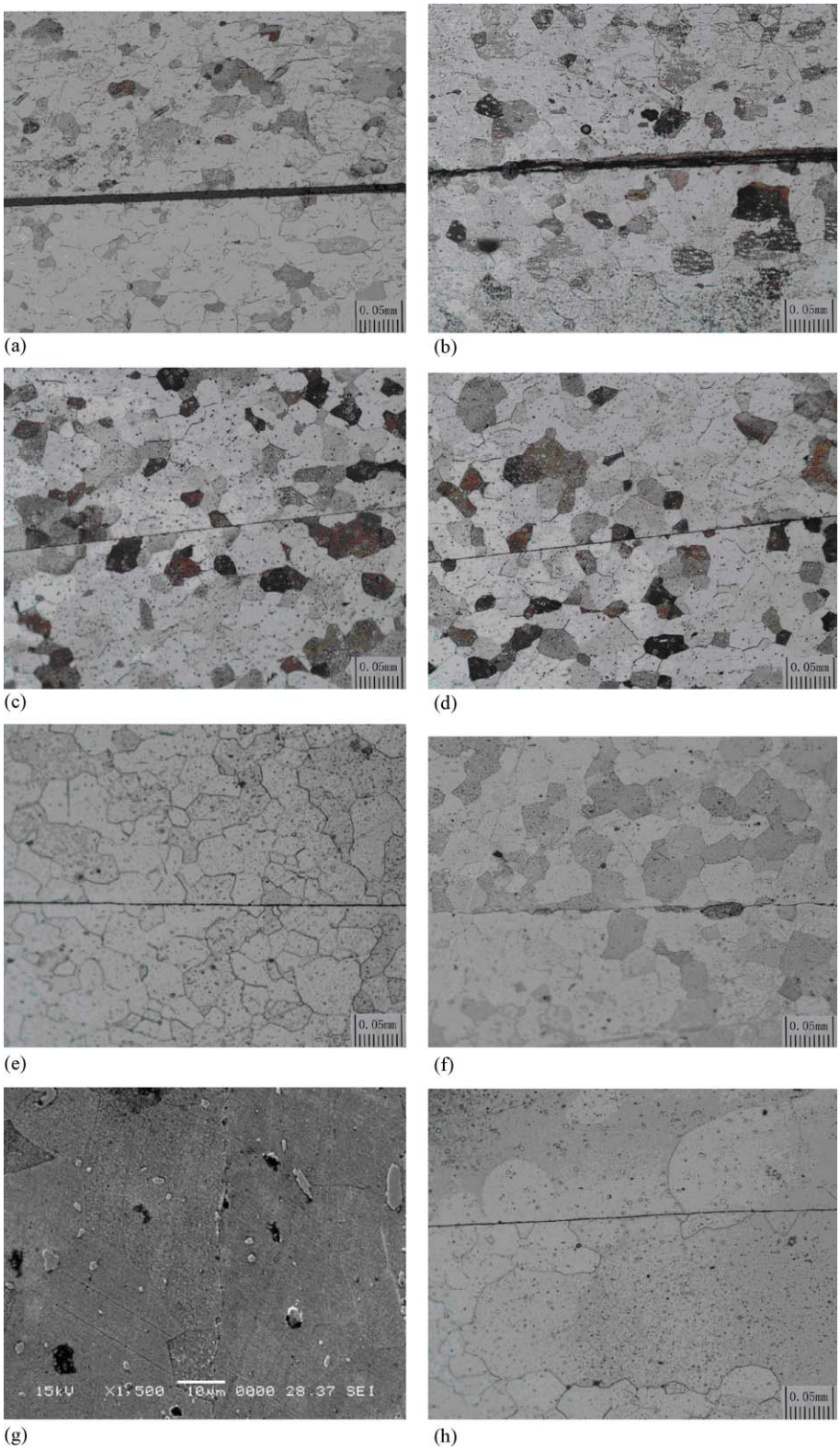

Fig. 5. Micrographs of the interface of the diffusion bonded zone for Fe–Cr–Al alloy: (a) 700 °C, 10 MPa, 1 h (×200); (b) 750 °C, 10 MPa, 1 h (×200); (c) 850 °C, 10 MPa, 1 h (×200); (d) 850 °C, 20 MPa, 1 h (×200); (e) 900 °C, 10 MPa, 1 h (×200); (f) 900 °C, 20 MPa, 1 h (×200); (g) 900 °C, 20 MPa, 1 h (×1500); (h) 1000 °C, 10 MPa, 1 h (×200).

shown in Fig. 5(a–e and h). At temperature of 700 and 750 °C, the bonding line is obviously presented on the interface, indicating nearly no formation of metallic bond. As temperature increases, the bonding line becomes narrow but still clear. An increase in temperature from 700 to 900 °C is accompanied with a slow growth in grain size, while a rapid increase occurs when the temperature increases from 900 to 1000 °C. As large grain results in a decrease of properties of bonded joints, the bonding

Table 1
Comparison of performance of $Cu/ZnO/Al_2O_3$ and Ce-doped catalyst coatings

Catalyst	Conversion 232 °C (%)	Conversion maximum (%)	T, 80% conversion (°C)	S_e minimum (%)[a]	S_e mean (%)[a]	CO maximum (vol.%)
Cu100	40.1	92.3	265	93.7	94.2	1.6
Cu100 [Ce10]	53.8	93.3	261	92.9	94.5	1.86
Cu70/Zn30	43.5	95.1	260	93.4	93.8	1.68
Cu70/Zn30 [Ce7]	54.8	96.8	256	91.9	94.0	2.05
Cu50/Zn50	38.3	90.4	271	93.5	94.2	1.68
Cu50/Zn50 [Ce5]	62.5	97.9	251	94.9	96.8	1.3
Cu40/Zn60	40.1	91.4	270	93.5	94.2	1.66
Cu40/Zn60 [Ce4]	44.5	90.5	258	93.8	96.7	1.60
Cu20/Zn80	20.6	72.3	–	93.6	94.3	1.65
Cu20/Zn80 [Ce2]	15.6	88.3	281	92.1	93.2	2.1

WHSV = 8.27 h^{-1}, $(n)H_2O/(n)CH_3OH$ = 1.3, temperature: 232–292 °C.
[a] S_e: carbon dioxide selectivity.

temperature should not be more than 1000 °C. With the bonding pressure increasing from 10 to 20 MPa, no obvious change in microstructure at 850 °C was observed as shown in Fig. 5(c and d). However, as shown in Fig. 5(e and f), the microstructure at 900 °C and 20 MPa shows no evidence of the bonding line and the grain boundary diffusion to each other's side near the interface can be detected. In Fig. 5(g), the percentage of bonded area is about 90% and some voids can be only occasionally observed on the interface. It has been widely accepted that too high bonding pressure results in large deformation, so the bonding pressure of 20 MPa is appropriate in the case. With the optimized bonding conditions of 900 °C and 20 MPa, the wedded microchannel reactor (Fig. 3) showed no leakage at an internal pressure of 1 MPa at 20 °C, which reveals that the sound sealing of a microchannel reactor can be successfully achieved.

3.2. Optimization of composition of catalyst coatings

The SRM activities of $Cu/ZnO/Al_2O_3$ and the corresponding Ce-doped catalyst coatings were compared in the range of reaction temperature from 232 to 292 °C. The results are summarized in Table 1. It is clear that Ce-doped materials are consistently more active and selective with the exception of the Cu20/Zn80 [Ce2]. As shown in Table 1, the Cu50/Zn50 [Ce5] generates the highest methanol conversion maximum, the highest methanol conversion at 232 °C, the lowest temperature of 80% methanol conversion, and the highest mean CO_2 selectivity. In other words, the Cu50/Zn50 [Ce5] is most active and selective. The effect of varying Ce loading at fixed Cu/Zn molar ratio of 1 is presented in Fig. 6. The highest methanol conversion was again observed by the Cu50/Zn50 [Ce5]. The carbon dioxide selectivity is similar and superior for the Cu50/Zn50 [Ce5] and Cu50/Zn50 [Ce2.5]. The Cu50/Zn50 [Ce15] gives the poorest performance with respect to conversion and selectivity at most temperatures. An increase in CeO_2 concentration means a decrease in the overall copper concentration in catalysts, consequently, a decrease in amount of Cu in activated catalysts. The overall effect is the existence of a maximum ratio, inferring that, beyond the concentration limit for CeO_2, its synergetic effect begins decreasing while its role as an active site for SRM reaction becomes significant. In comparison with copper species, CeO_2 is less active if used solely as a catalyst. Therefore, the optimized catalyst coating is Cu50/Zn50 [Ce5].

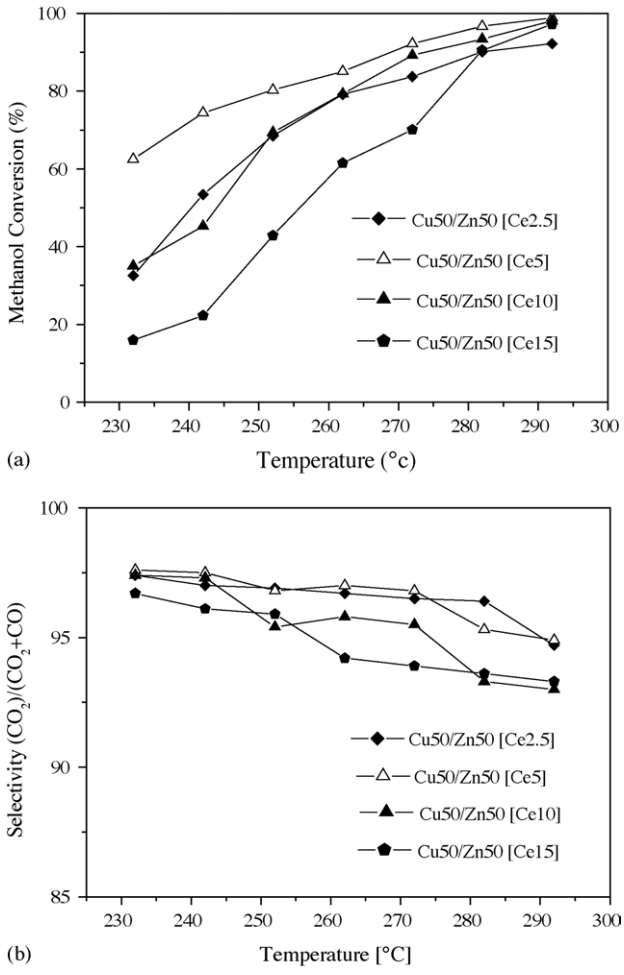

Fig. 6. Effect of Ce loading for Ce-doped catalyst coatings: (a) methanol conversion and (b) carbon dioxide selectivity ($(n)H_2O/(n)CH_3OH$ = 1.3, WHSV = 8.27 h^{-1}).

3.3. Characterization of the catalyst coating

Fig. 7 shows SEM images of γ-Al_2O_3 coatings on the Fe–Cr–Al alloy. The denotations of (1) and (2) stand for γ-Al_2O_3 coating and Fe–Cr–Al alloy, respectively. It shows that the adherence of γ-Al_2O_3 coating on the Fe–Cr–Al alloy is very good, without detachment or uncovered areas.

Fig. 8 shows in situ X-ray diffraction patterns taken during temperature-programmed reduction (TPR) of Cu50/Zn50 and Cu50/Zn50 [Ce5]. The evolution of the intensity of the Cu(1 1 1) line affords the onset and extent of reduction while the evolution of the crystallite size is obtained from the line width. For the two samples, crystalline Cu began to appear as the temperature increased to 150 °C and eventually no crystalline CuO was detected after reduction at 280 °C. It is interesting to note that some Cu_2O was observed in the Cu50/Zn50 [Ce5] during reduction at 250 °C and diminished with increasing temperature. It is most likely that the redox equilibrium shown in Eq. (4) (electronic exchange) can form between the CeO_2 and Cu species and Cu^+ species may exist in Ce-doped catalyst coatings at some temperature during

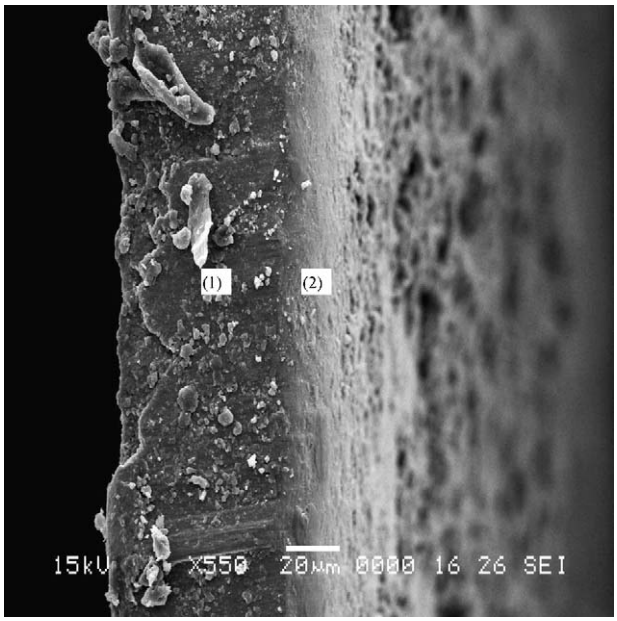

Fig. 7. SEM of γ-Al_2O_3 coating on the thermally treated metal.

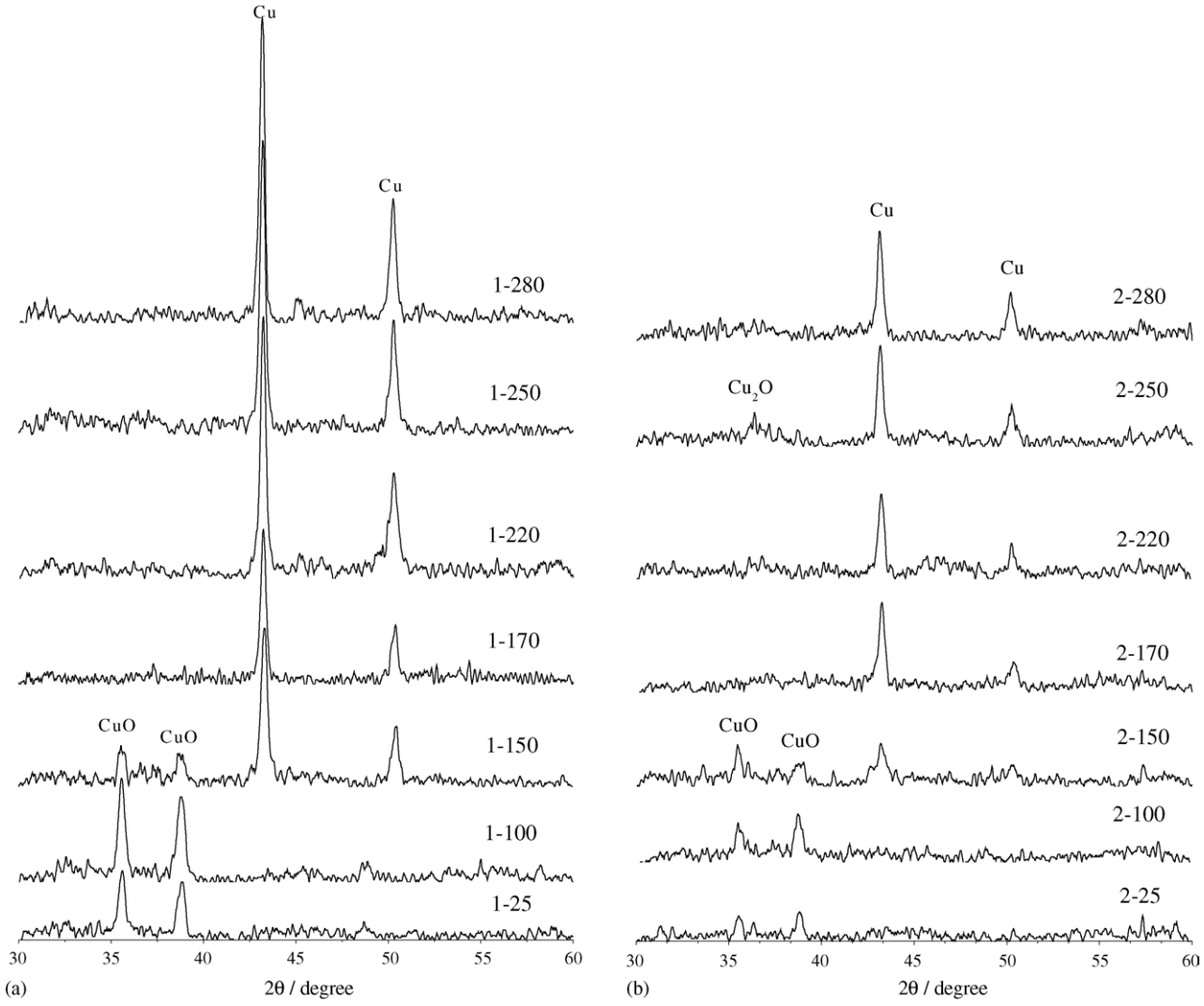

Fig. 8. In situ XRD: (a) Cu50/Zn50 and (b) Cu50/Zn50 [Ce5].

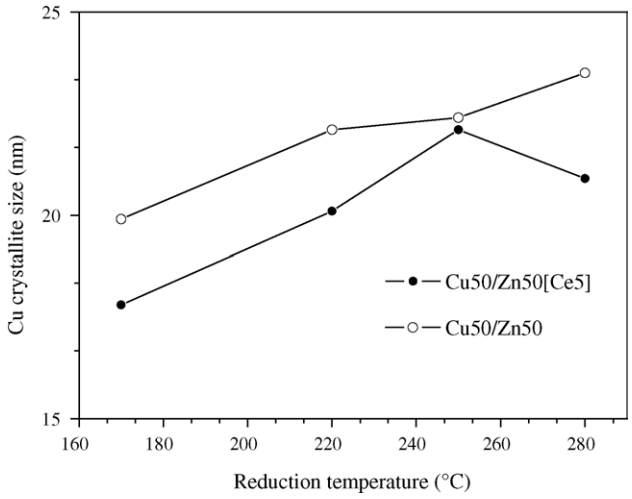

Fig. 9. Evolution of Cu crystallite size during TPR: (a) Cu50/Zn50 and (b) Cu50/Zn50 [Ce5].

reduction:

$$Ce^{4+} + Cu \rightarrow Ce^{3+} + Cu^{+} \quad (4)$$

The evolution of the Cu crystallite size during TPR is shown in Fig. 9. The Cu crystallite appears to grow with increase in the temperature of reduction. The exception to this trend is Cu50/Zn50 [Ce5] with a maximum at 250 °C, which is likely attributed to the presence of Cu_2O as shown in Fig. 8. It can be conclude that doping of Ce results in a decrease in Cu crystallite size at all temperatures during TPR by comparing the two figures shown in Fig. 9, which is in full agreement with the followed results of Cu surface area measurements.

XPS experiments have been carried out before and after exposure of the Cu50/Zn50, Cu50/Zn50 [Ce5] and Cu100 [Ce10] to SRM conditions in order to investigate the influence of composition on the copper oxidation state. The results are shown in Fig. 10 and Table 2. For the outgassed fresh catalysts, Cu $2p_{3/2}$ peaks are centered between 934.6 and 934.8 eV, which may be related to a $CuAl_2O_4$ spinel from the aluminium-containing

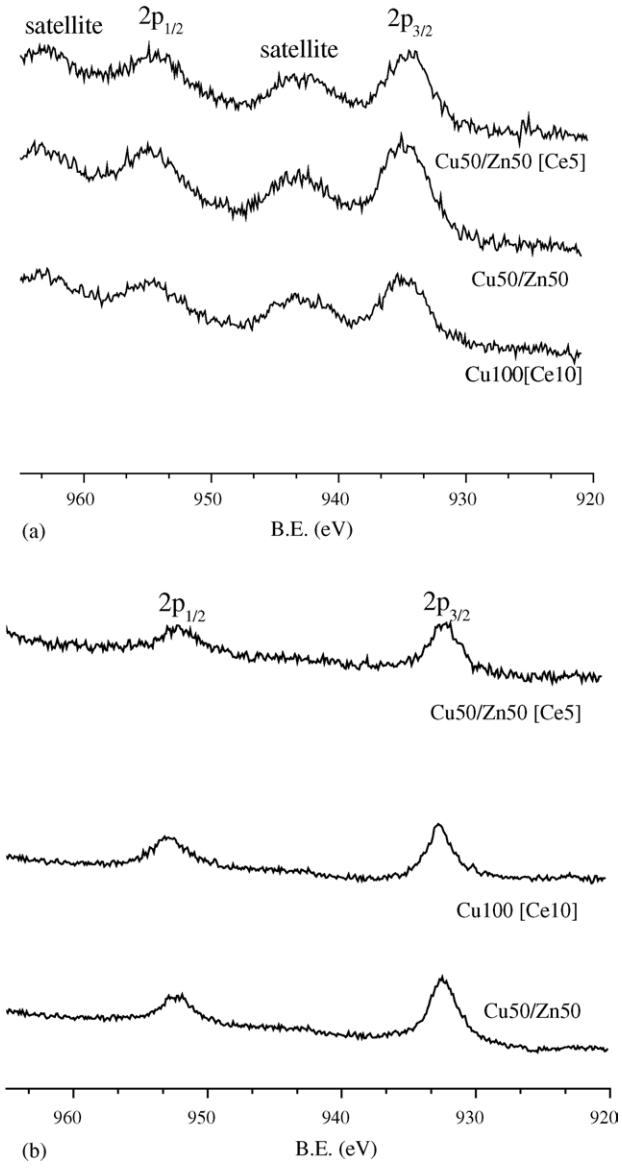

Fig. 10. XPS spectra of Cu 2p region for Cu50/Zn50, Cu100 [Ce10], and Cu50/Zn50 [Ce5] (a) after calcinations and (b) after reaction.

Table 2
XPS results for Cu50/Zn50, Cu50/Zn50 [Ce5], Cu100 [Ce10] after calcination and reaction

Catalyst name	Treatment history	Peak	BE (eV)	α_A (eV)
Cu50/Zn50 [Ce5]	Calcined	Cu $2p_{3/2}$	934.8	1851.2 1852.1 1852.8
	Post reaction	Cu $2p_{3/2}$	932.4	1848.8 1849.7 1850.9
Cu100 [Ce10]	Calcined	Cu $2p_{3/2}$	934.7	1851.1 1852 1852.9
	Post reaction	Cu $2p_{3/2}$	932.6	1848.8
Cu50/Zn50	Calcined	Cu $2p_{3/2}$	934.6	1851.7
	Post reaction	Cu $2p_{3/2}$	932.2	1851.4

catalysts [16]. Also the Cu^{2+} satellite peak is observed at ca. 943 eV. As shown in Fig. 10(b), the Cu $2p_{3/2}$ signals of the three catalysts shift down to between 932.2 and 932.6 eV after reaction, which may be assigned to either Cu^0 or Cu^+. On the other hand, as little shake-up feature is observed in the Cu 2p spectrum (Fig. 10(b)), it is most likely that Cu^{2+} is not present on the surface of the three catalysts. As the binding energies of both Cu^0 and Cu^+ species are quite similar to differentiate which of these species are present in the catalysts, the modified Auger parameter was calculated [17,18]. Typical values of this parameter around 1851.3 and 1849.5 eV were found for Cu^0 and Cu^+ species, respectively. As shown in Table 2, the α_A value of 1851.4 eV for the Cu50/Zn50 clearly indicates that copper is in Cu^0 state on the catalyst coating surface. For the Cu50/Zn50 [5], the α_A values are 1848.8, 1849.7, and 1850.9 eV, which are related to Cu^+ and Cu^0. For the Cu100 [Ce10], the α_A value of

Table 3
Physical properties and TOFs for SRM over various catalyst coatings

Catalyst	MeOH[a] conversion (%)[a]	BET surface area ($m^2\ g^{-1}$)	Pore volume ($mL\ g^{-1}$)	Pore radius (Å)	Cu surface area[b] ($m^2\ g^{-1}$)[b]	TOF[b] (s^{-1})[c]
Cu50/Zn50	38.3	174	0.36	73.2	9.4	0.406
Cu50/Zn50 [Ce5]	62.5	172	0.35	74.6	11.2	0.633
Cu100 [Ce10]	53.8	168	0.38	73.6	6.8	0.411

[a] WHSV = 8.27 h^{-1}, $(n)H_2O/(n)CH_3OH = 1.3$, $T = 505$ K.
[b] Measured by N_2O absorption.
[c] Hydrogen molecules produced per surface copper atom per second.

1848.8 eV indicates that Cu^+ is the predominant species. The XPS results clearly show that Cu^+ species is present on the surface of the Ce-doped catalyst.

The physical properties and TOF values at 505 K for the representative catalyst coatings are summarized in Table 3. It is clear that Cu50/Zn50 [Ce5] exhibits higher Cu surface area than Cu50/Zn50, which correlates well with the results of in situ XRD in Fig. 9. As it is well-known that large number of surface sites of Cu is favorable for the rate of SRM [19,20], the high activity of Cu50/Zn50 [Ce] can be partly attributed to the presence of the highly dispersed Cu crystallite resulting from doping of Ce. As shown in Table 3, with the similar values of BET, pore volume and pore radius for the three catalyst coatings, the Cu50/Zn50 [Ce5] exhibits highest TOF value. For SRM reaction, the reaction efficiency strongly depends on the amount of Cu^+ species formed in catalysts [21]. Idem and Bakhshi [22] suggested that superior catalytic activity in the steam reforming of methanol was attributed to the formation of an optimum Cu^0–Cu_2O combination on the catalyst. Breen et al. [23] have reported that the steam reforming of methanol was carried out through methoxy, formate, and formaldehyde species. It was likely that methoxy, formate, and formaldehyde species were adsorbed on the surface of Cu^0, and the role of Cu^+ may be stabilization of any oxygenates near the Cu^+ sites [24]. From the XPS results in Table 2, both Cu^0 and Cu^+ exist on the surface of the Cu50/Zn50 [Ce5], indicating the presence of synergetic effect of Cu^0 and Cu^+ on the coating surface. As only Cu^0 and Cu^+ appearing on the surface of Cu50/Zn50 and Cu100 [Ce10], respectively, the highest TOF value of Cu50/Zn50 [Ce5] is most likely due to the synergetic effect of Cu^0 and Cu^+ on the coating surface. This may be the other reason for the superior activities of the Cu50/Zn50 [Ce5].

3.4. Performance of the microchannel reactor

The effect of reaction temperature on the performance of the microchannel reactor with the Cu50/Zn50 [Ce5] catalyst is shown in Fig. 11. Methanol conversion and hydrogen yield increase with increasing temperature. The maximum methanol conversion is 92.2% at 292 °C. In the temperature range of 242–292 °C, the outlet CO concentration averages at 1.11% with the minimum of 0.87% at 282 °C. Many reports indicate that CO is produced by the reverse water shift reaction (Eq. (3)) at a higher temperature. Because this reaction is endothermic, higher temperature is favorable for the production of CO. In our experiment, the outlet CO concentration fluctuates with increasing reaction temperature, which is different from the results of pellet type catalysts in a conventional fixed-bed reactor [25]. In our opinion, it is most likely that the differences between fixed-bed reactors and microchannel reactors in mass transfer, heat transfer, and flow pattern result in the fluctuation. Further experiments are being carried out to reveal the cause.

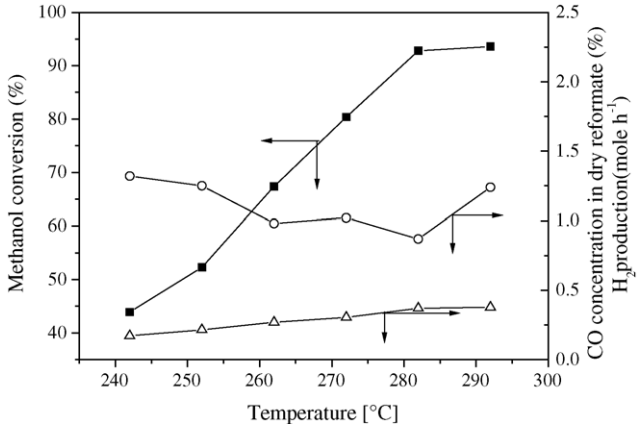

Fig. 11. Effect of temperature on catalytic activity (feed flow rate = 6 $cm^3\ h^{-1}$ $(n)H_2O/(n)CH_3OH = 1.3$).

Fig. 12 shows the effect of space velocity on the performance of the microchannel reactor with the catalyst coating of Cu50/Zn50 [Ce5]. Methanol conversion and the outlet CO conversion decrease with an increase in feed flow rate from 6 to 30 $cm^3\ h^{-1}$ at 272 °C. The increase in feed flow rate means the increase in space velocity and the decrease in contact time.

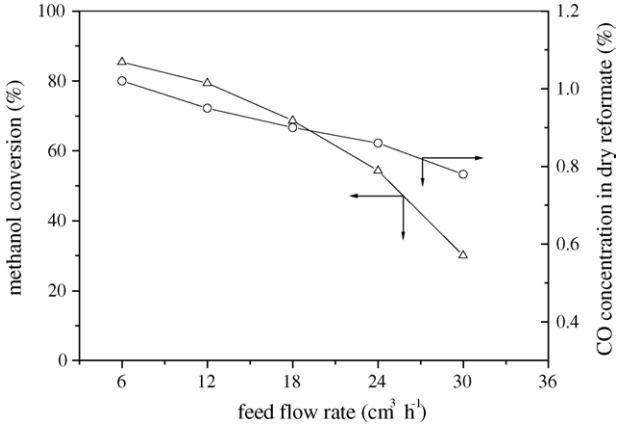

Fig. 12. Effect of feed flow rate on catalytic activity ($T = 272$ °C, $(n)H_2O/(n)CH_3OH = 1.3$).

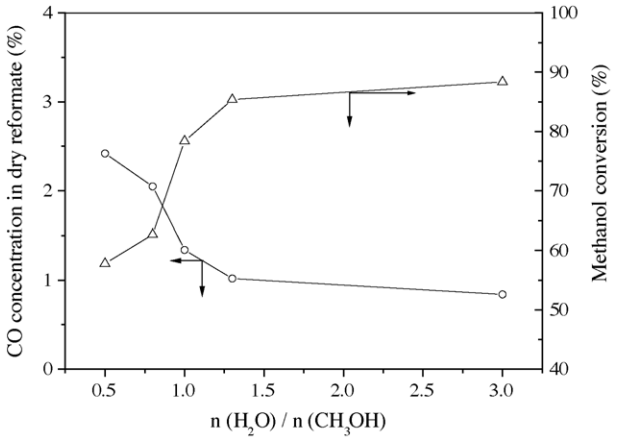

Fig. 13. Effect of H_2O/CH_3OH molar ratio on catalytic activity ($T = 272\,^{\circ}C$, feed flow rate = 6 $cm^3\,h^{-1}$).

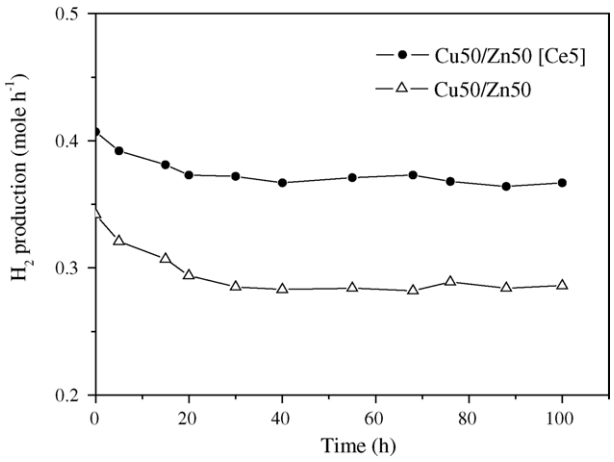

Fig. 14. Effect of reaction time on the performance of microchannel reactor with the catalyst of Cu50/Zn50 [Ce5] and Cu50/Zn50 ($T = 282\,^{\circ}C$, $(n)H_2O/(n)CH_3OH = 1.3$, feed flow rate = 6 $cm^3\,h^{-1}$).

Although there are lots of debates [26] on the mechanism of CO formation and selectivity, it is the same that CO in dry reformate decreases with an decrease in contact time.

The effect of H_2O/CH_3OH molar ratio on the performance of the microchannel reactor with the catalyst of Cu50/Zn50 [Ce5] is presented in Fig. 13. It can be seen that methanol conversion increases remarkably with an increase in H_2O/CH_3OH molar ratio below 1.0 at 272 °C with feed flow rate of 6 $cm^3\,h^{-1}$, while the increase slows down beyond the ratio of 1.0. As shown in Fig. 13, the outlet CO concentration decreases with an increase in H_2O/CH_3OH molar ratio. An outlet CO concentration in dry reformate of about 2.05% is determined when the H_2O/CH_3OH molar ratio is 0.8, and the outlet CO concentration in dry reformate decreases to 1.02% with increasing H_2O/CH_3OH molar ratio up to 1.3. The results show that higher H_2O/CH_3OH molar ratio is favorable for reducing the outlet CO concentration. According to Eq. (1), the H_2O/CH_3OH molar ratio in the 1.0 will be stoichiometrically optimum value in SRM reaction. However, it is known from Eqs. (1) and (3) that excess H_2O promotes methanol conversion and reduces CO concentration by shifting the WGS equilibrium towards the right. Because more H_2O in mixed H_2O and CH_3OH solution gives rise to the burden of heating and elimination process, the ratio between 1.3 and 1.5 is reasonable.

In order to investigate the stability of the performance of the microchannel reactor, the continuous operation has been performed for 100 h over catalysts of the Cu50/Zn50 [Ce5] and Cu50/Zn50 in the condition as follows: the temperature of 282 °C, feed flow rate of 6 $cm^3\,h^{-1}$, and the molar ratio of water to methanol of 1.3. The results are shown in Fig. 14. It can be seen Cu50/Zn50 catalyst deactivates rapidly before 20 h and hydrogen production decreases from 0.342 to 0.285 mol h^{-1}, approximately a decrease of 16.7%. There is also an initial deactivation of the Cu50/Zn50 [Ce5] catalyst and the hydrogen production decreases from 0.41 to 0.37 mol h^{-1}, approximately a decrease of 9.8%. After about 20 h, H_2 yield, methanol conversion and CO concentration are stable throughout the period at about 0.285 mol h^{-1}, 74.2 and 1.61 mol% for Cu50/Zn50 catalyst, respectively. The corresponding values after 15 h for Cu50/Zn50 [Ce5] are 0.37 mol h^{-1}, 90.2 and 0.87%, respectively. The results clearly show that CeO_2 improves both the activity and stability of the catalysts. It is important to note that a low-temperature shift step must be implemented prior to the CO clean-up step for catalysts yielding CO concentrations above 1 mol% [27]. To spare the available space, it is highly undesirable to have to install additional clean-up units. The CO content of the Cu50/Zn50 [Ce5] catalyst is 0.87 mol% in the conditions as mentioned above, which can well meet this demand. Assuming 60% efficiency of fuel cell and 80% utilization of H_2, H_2 yield of 0.37 mol h^{-1} of Cu50/Zn50 [Ce5] means the estimated power output is about 11 W [28].

4. Conclusions

Preparation of a microchannel reactor concerning SRM has been investigated by optimizing the composition of catalyst coatings and parameters of diffusion bonding. It was found that the bonding temperature and pressure have important influences on the percentage of bonded area. The optimum parameters are temperature of 900 °C and pressure of 20 MPa. The comparison in catalytic activities between $Cu/ZnO/Al_2O_3$ and the corresponding Ce-doped ones indicates that CeO_2 has an important influence on improving catalytic activity, decreasing the outlet CO concentration, strengthening stability. Based on the results of the characterization of catalyst coatings, it can be attributed to the presence of the highly dispersed Cu crystallite and to the synergetic effect of Cu^0 and Cu^+ on the surfaces of the coatings. The bonded microchannel reactor with the optimum catalyst coating of Cu50/Zn50 [Ce5] has been investigated at various operating conditions. The results of continuous 100 h operation show the developed microchannel reactor can produce enough hydrogen for a power output of 11 W.

References

[1] G. Cacciola, V. Antonucci, S. Freni, J. Power Sources 100 (2001) 67–79.

[2] Y. Tanaka, T. Utaka, R. Kikuchi, K. Sasaki, et al., Appl. Catal. A 238 (2003) 11–18.
[3] G. Park, D.J. Seo, S.-H. Park, et al., Chem. Eng. J. 101 (2004) 87–92.
[4] P. Reuse, A. Penken, K. Hass-Santo, et al., Chem. Eng. J. 101 (2004) 133–141.
[5] D. Gobby, I. Eames, A. Gavriilidis, A vertically averaged formulation of wall catalytic reactions in microchannel flows: single isothermal and non-isothermal reactions, in: Proceedings of the Fifth International Conference of Microreaction Technology, Strasbourg, 2001, pp. 142–149.
[6] A.Y. Tonkovich, J.L. Zika, M.J. LaMont, et al., Chem. Eng. Sci. 54 (1999) 2947–2951.
[7] V. Hessel, W. Ehrfeld, K. Golbig, et al., Gas/liquid microreactors for direct fluorination of aromatic compounds using elemental fluorine, in: Proceedings of the Third International Conference of Microreaction Technology, Frankfurt, 2000, pp. 526–540.
[8] A. Rouge, B. Spoetzl, S. Schenk, et al., Chem. Eng. Sci. 56 (2001) 1419–1427.
[9] A. Rouge, A. Renken, Forced periodic temperature oscillations in microchannel reactors, in: Proceedings of the Fifth International Conference of Microreaction Technology, Strasbourg, 2001, pp. 230–239.
[10] P. Pfeifer, K. Schubert, M.A. Liauw, et al., Appl. Catal. A 270 (2004) 165–175.
[11] S.P. Ashok, G.D. Terry, S. Nicholas, et al., J. Power Sources 136 (2004) 220–225.
[12] G.W. Chen, Q. Yuan, H.Q. Li, et al., Chem. Eng. J. 101 (2004) 101–106.
[13] K. Haas-Santo, M. Fichtner, K. Schubert, Appl. Catal. A 220 (2001) 79–92.
[14] Th. J. Osinga, B.G. Linsen, W.P. van Beek, J. Catal. 7 (1967) 227–235.
[15] J.W. Evans, M.S. Wainwright, A.J. Bridgewater, D.J. Young, Appl. Catal. 7 (1983) 75–83.
[16] B.R. Strohmeier, D.E. Leyden, R.S. Field, et al., J. Catal. 94 (1985) 514–530.
[17] C.D. Wagner, L.H. Gale, R.H. Raymond, Anal. Chem. 51 (1979) 466–469.
[18] M. Fernández-García, E.G. Rebollo, G.A. Ruiz, et al., J. Catal. 172 (1997) 146–159.
[19] R.G. Herman, K. Klier, G.W. Simmons, et al., J. Catal. 56 (1979) 407–429.
[20] B. Lindström, J. Lars, P. Pettersson, et al., Appl. Catal. A 234 (2002) 111–125.
[21] L.Y.T. Hayakawa, K. Suznki, et al., Appl. Catal. A 223 (2002) 137–145.
[22] R.O. Idem, N.N. Bakshi, Ind. Eng. Chem. Res. 33 (1994) 2056–2065.
[23] J.P. Breen, F.C. Meunier, J.R.H. Ross, Chem. Commun. 22 (1999) 2247–2248.
[24] T. Fujitani, M. Saito, Y. Kanai, T. Kakumoto, et al., Catal. Lett. 25 (1994) 271–278.
[25] X.R. Zhang, P.F. Shi, J. Mol. Catal. A 194 (2003) 99–105.
[26] H. Purnama, T. Ressler, R.E. Jentoft, et al., Appl. Catal. A 259 (2004) 83–94.
[27] B. Lindström, L.J. Pettersson, J. Power Sources 106 (2002) 264–273.
[28] G. Park, D.J. Seo, S.-H. Park, et al., Chem. Eng. J. 101 (2004) 87–92.